



Structural and Functional Imaging of Normal Bone Marrow and Evaluation of Its Age-Related Changes

Judy S. Blebea, MD,¹ Mohamed Houseni, MD,¹ Drew A. Torigian, MD, MA, Chengzhong Fan, MD, Ayse Mavi, MD, Ying Zhuge, PhD, Tad Iwanaga, BSc, Shipra Mishra, BSc, Jay Udupa, PhD, Jiyuan Zhuang, Rohit Gopal, and Abass Alavi, MD

A number of noninvasive imaging techniques have been used for the evaluation of bone marrow, including magnetic resonance imaging (MRI) and bone marrow scintigraphy. The appearance of bone marrow on MRI varies considerably depending on the proportion of red and yellow marrow, and the composition of the red marrow and its distribution with relation to age and sex. The composition of bone marrow also can vary under physiological and pathological conditions. MRI is a highly sensitive technique for evaluating the bone marrow, but it is limited in its practical use for whole-body bone marrow screening. Bone marrow scintigraphy with radiolabeled compounds such as technetium-99m-labeled nanocolloid and monoclonal antibodies has the advantage of evaluating the entire bone marrow, and has been used for the diagnosis of various bone marrow disorders. In addition, ¹⁸F-fluorodeoxyglucose positron emission tomography (FDG-PET) imaging can be used to evaluate bone marrow metabolism and disease and to provide information about the state of the primary tumor, lymph nodes, and distant metastases. Understanding of the appearance of normal bone marrow, including age- and sex-specific differences with each of these imaging modalities, is essential to permit accurate diagnosis of benign and malignant bone marrow disorders. We present a review of MRI and scintigraphy of normal bone marrow with some emphasis on FDG-PET imaging in assessing marrow activity in normal and abnormal states and also present preliminary data regarding normal age-related changes in bone marrow through use of FDG-PET, as well as the role of segmentation of bone marrow on MRI for quantitative calculation of the metabolic volumetric product for red marrow metabolism using FDG-PET.

Semin Nucl Med 37:185-194 © 2007 Elsevier Inc. All rights reserved.

To date, several useful techniques, such as bone marrow aspiration and biopsy, magnetic resonance imaging (MRI), and bone marrow scintigraphy have been used for the evaluation of bone marrow in clinical practice. Among them, bone marrow biopsy is an excellent procedure, is the commonest technique for evaluating bone marrow, and provides a specific diagnosis. However, the procedure is invasive and is limited by sampling error.¹

MRI is a highly sensitive technique for the evaluation of bone marrow. Bone marrow can be affected by a number of benign and malignant processes; therefore, a thorough understanding of the MRI appearance of normal bone marrow and its patterns

of distribution in the osseous structures and causes of marrow disease is essential to accurately detect abnormal states. Radionuclide bone marrow scintigraphy is another simple noninvasive technique that has been used to evaluate for marrow disease. Several radiotracers have been developed that can target the reticuloendothelial system, erythropoietic cells, and granulopoietic cells, permitting evaluation of the whole-body distribution of red marrow and the diagnosis of several disorders.^{2,3} A new emerging technique for assessment of bone marrow is whole-body ¹⁸F-fluorodeoxyglucose positron emission tomography (FDG-PET), which can provide information about functioning normal bone marrow and its physiologic distribution as well as allow for the detection of pathologic lesions with increased glucose metabolism.

Department of Radiology, University of Pennsylvania School of Medicine, Philadelphia, PA.

¹J.S.B. and M.H. contributed equally to the work (co-lead authors).

Address reprint requests to Abass Alavi, MD, Department of Radiology, Division of Nuclear Medicine, Hospital of the University of Pennsylvania, 1 Donner Building, 3400 Spruce Street, Philadelphia, PA 19104-4283. E-mail: Abass.Alavi@uphs.upenn.edu

Bone Marrow Constituents

Bone is a highly differentiated connective tissue that allows for the mechanical support of muscles and functions for

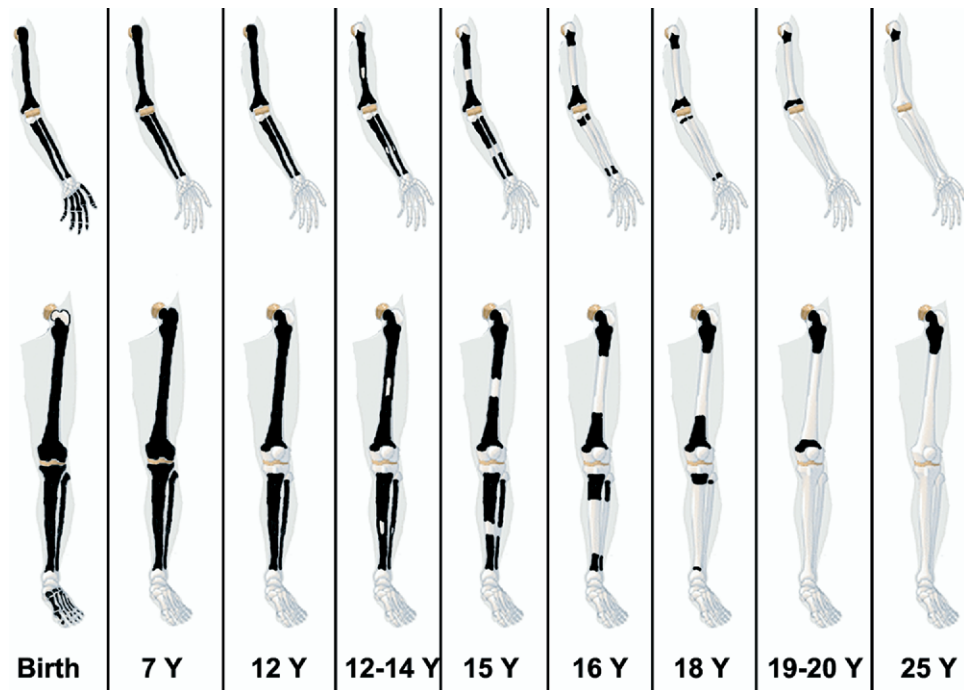


Figure 1 Diagrammatic representation of the amount and distribution of red marrow in tubular bones from birth until 25 years. At birth, unossified epiphyses do not contain red marrow. (Color version of figure is available online.)

hematopoiesis, the immune system, coagulation, and calcium and phosphorus metabolism among others.² The majority of the medullary cavity of bone is composed of bone marrow, with only approximately 15% being trabecular bone.⁴ The amount of fat and nonfat components of bone marrow is altered with age, with a normal physiologic progressive conversion of red to yellow marrow in the peripheral skeleton and a progressive increase in the proportion of fat cells in the axial skeleton over time, accounting for the age-related change in red marrow distribution and composition.

At birth, virtually all marrow is hematopoietic. During fetal growth, hematopoiesis takes place in all skeletal compartments as well as in the liver and spleen. Before birth, splenic and hepatic hematopoiesis disappears. Red to yellow marrow conversion typically begins in the distal phalanges and proceeds in a centripetal fashion, with the adult pattern of marrow distribution generally achieved by the age of 25, when the red marrow is distributed primarily in the axial skeleton, sternum, ribs, and proximal femora and humeri (Fig. 1). In individual long bones, such as the tibia and femur, conversion begins in the diaphysis and progresses both distally and proximally within the bone, although conversion to the distal end is more rapid.^{5,6} Persistent isolated or confluent islands of hematopoietic marrow may remain within the medullary cavity of the long bones. Overall, marrow conversion progresses at a slower rate in adulthood.⁷

Adult bone marrow volume is approximately 50% yellow marrow located predominantly in the appendicular skeleton and 50% red marrow located primarily in the axial skeleton and proximal aspect of the limbs (Fig. 2).^{3,8} Yellow marrow contains approximately 95% fat cells and 5% nonfat cells

whereas red marrow comprises 60% hematopoietic cells and 40% fat cells.⁹ The 3 major components of the red marrow are hematopoietic (erythropoietic and myelopoietic) cells, reticuloendothelial cells, and a trabecular framework that supports both cell types. The proportion of fat and nonfat cells influences the signal intensity of the bone marrow and hence its appearance on MRI. Nerves and vascular sinusoids also course throughout the hematopoietic marrow. Bone marrow normally weighs approximately 3,000 g in adult men and 2,600 g in adult females. However, because approximately one half of the red marrow, by weight, is adipose tissue, approximately 75% of the total marrow weight in adults is composed of adipose tissue.¹⁰

In addition, the bone marrow has a dual blood supply consisting of a periosteal capillary network and a nutrient artery that penetrates the cortex and branches within the myeloid tissue. The estimated blood flow through the bone marrow, as assessed with PET and a ¹⁵O-labeled CO₂ steady-state technique, is approximately 10 mL/min/100 cm³ in healthy adults.¹¹

Benign bone marrow hyperplasia is found in association with long-distance running, smoking, and obesity and is more common in females than males. Benign bone marrow hyperplasia has been reported in 9.7% to 35% of the healthy population and generally is seen as an increase in red marrow within the distal metaphyseal region of the humerus or femur or within the proximal metaphyseal region of the tibia.¹²⁻¹⁴ When there are additional demands for hematopoiesis, as seen with chronic anemia or red marrow replacement by fibrosis or malignant processes, the reconversion of yellow to red marrow occurs in a reverse pattern relative to conversion.

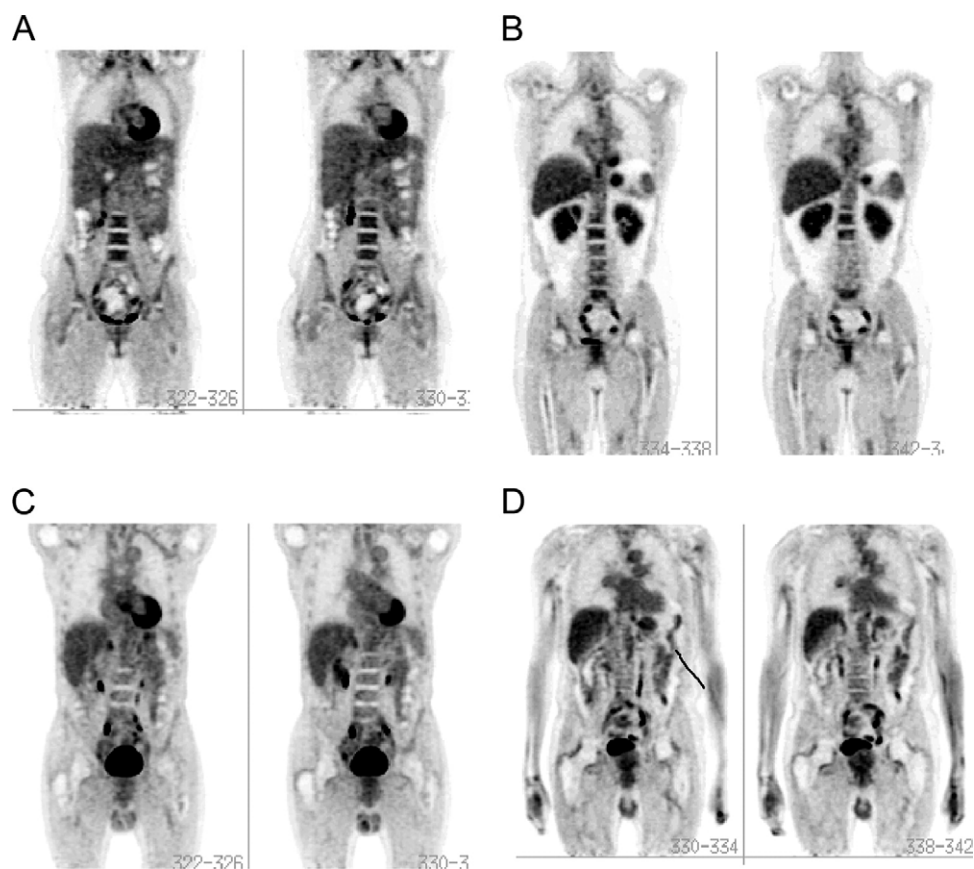


Figure 2 Whole-body FDG-PET images of subjects at different ages: younger than 20 years (A), at 35 years (B), at 55 years (C), and at 75 years (D). Note that red marrow activity and distribution in the spine, pelvic bones, and femora are more prominent in younger age.

MRI of Normal Bone Marrow

MRI is a highly sensitive technique for imaging of normal and abnormal marrow. The MR appearance of bone marrow is strongly influenced by the proportion of fat present. Fat protons are bound in hydrophobic CH_2 groups of relatively heavy molecular complexes that permit efficient spin-lattice relaxation and a short T1 relaxation time, leading to increased T1-weighted signal intensity.¹⁵⁻¹⁷ The spin-spin relaxation of fat protons, however, results in a relatively long T2 relaxation time with associated increased signal intensity on T2-weighted images. The signal intensity of red marrow depends on the proportion of fat protons to water protons, and is lower than that of yellow marrow but higher than that of muscle with the contrast between red and yellow marrow most apparent on T1-weighted and fat suppressed sequences.

The signal intensity of red marrow is variable on gradient echo images. On opposed phase gradient echo images, the net difference between water and fat proton magnetizations, which affects the voxel signal intensity, typically approaches zero as there are usually equivalent amounts of water and fat in red marrow. However, if there are increased amounts of fat as in yellow marrow or increased amounts of water as in infiltrated red marrow, the marrow signal will remain elevated.^{12,18}

Fat suppression sequences are routinely used to null the signal intensity from fat and increase the conspicuity of pathologic marrow lesions. Short inversion-time-inversion-recovery (STIR) sequences have been used to null the signal of fat protons, allowing for greater conspicuity of pathologic lesions and uninvolved bone marrow. STIR images have a reduced signal-to-noise ratio but are less susceptible to motion artifact as the signal from fat is suppressed. Chemical shift selective fat suppression also is used frequently in conjunction with T2-weighted fast spin echo imaging but is susceptible to magnetic field inhomogeneities especially with large fields of view.

Patterns of normal bone marrow distribution on MRI in the spine were reported by Ricci and colleagues.¹⁹ With pattern 1, the vertebral body has uniformly low signal intensity except for some regions near the basivertebral vein; with pattern 2, there are band-like and triangular areas of high signal found in the periphery near the endplates and anteriorly and posteriorly at the corners of the vertebral bodies; pattern 3 is characterized by diffusely distributed areas of high signal intensity consisting of either numerous indistinct dots or fairly well-margined areas. In the lumbar spine, most of the patients with pattern 1 were younger than 30 years old, and there was a monotonic increase in patterns 2 and 3 with age.

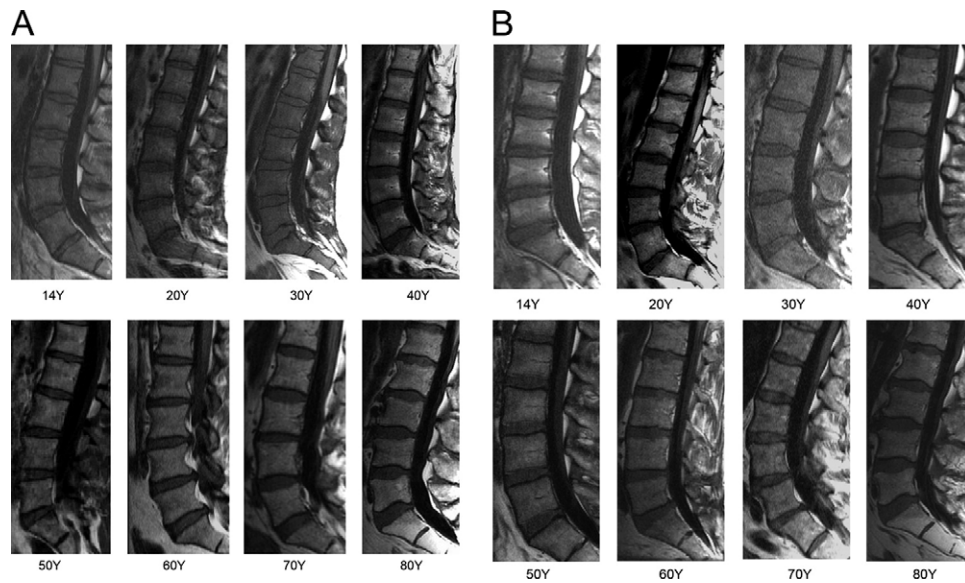


Figure 3 Sagittal T1-fluid-attenuated inversion recovery MR images through lumbar spine in subjects of different age in both women (A) and men (B). Note increase in high signal intensity fat content in vertebral bone marrow with age.

Duda and coworkers used chemical shift techniques to demonstrate that there is lower fat content in the marrow of the sacral vertebral bodies when compared with the lateral masses of the sacrum in both males and females and attributed this finding to the peripheral-to-central orientation of marrow conversion.²⁰ In addition, they found a higher level of signal intensity in the yellow marrow of the lateral masses in men than in women and a significantly greater proportion of sacral nonfatty marrow in women than men.²⁰ Mitchell and coworkers did report statistically significant sex-related differences in intertrochanteric marrow composition among healthy persons younger than 50 years of age, with a greater proportion of hematopoietic marrow in women than in men.²¹ Ishijima and colleagues evaluated the water fraction of lumbar vertebral bone marrow estimated from chemical shift misregistration on MRI and noted that the water fraction was significantly greater in reproductive-age women than in men of corresponding age.²² Kugel and coworkers, using MR spectroscopy, demonstrated that the relative proportion of fat in the vertebral bone marrow increases with age from 24% in those ages 11 to 20 years to 54% in those of age ≥ 61 years but is less in female subjects than male subjects in the same age groups (Fig. 3).²³ Other studies have failed to show a significant sex-related difference in vertebral marrow composition in the lumbar spine of healthy patients. Dooks and coworkers reported that the values for T1 and T2 relaxation times of the bone marrow of the lumbar vertebral bodies were slightly greater for women than men, but this value was not statistically significant. However, the measurements of T1 and T2 relaxation times did show a progressive and statistically significant decrease in mean values according to age for their patient population.²⁴ According to quantitative histological studies, the mean percentage volume of hematopoietic marrow in adults decreases progressively with age, comprising 29.2% in the eighth decade of life as compared with 57.9% in the first decade.²⁵

The enhancement of normal marrow in the adult after the intravenous administration of a gadolinium chelate is usually barely perceptible, although a measurable increase in signal intensity can be calculated if a region of interest is applied to ascertain signal intensity values.²⁶ Montazel and coworkers noted that the maximum percentage of enhancement of bone marrow in the thoracolumbar spine with ultrafast dynamic MRI was significantly related to age, with greater values in patients younger than 40 years compared with those ages 40 and older and also noted that the maximum percentage of enhancement decreased as fat content increased.²⁷ Performance of precontrast and postcontrast T1-weighted fat suppressed imaging with subsequent application of image subtraction techniques also can aid in the detection of abnormal marrow enhancement. Enhancement of the marrow caused by hypervascularity, increased marrow cellularity, and the presence of an extensive extravascular space that allows for contrast agent to pool can be seen in young children.²⁸ In fact, whole-body MRI has been performed in young adults and children to assess bone marrow metastasis in its entirety throughout the skeletal system.²⁹ However, the practical use of MRI for this purpose is limited.

Radiotracer-Based Bone Marrow Imaging

Radionuclide bone marrow scan (BMS) is a simple noninvasive technique that provides information about the whole-body distribution of functioning red bone marrow in various clinical states and also aids in the differential diagnosis of various disorders.³⁰⁻³² Since the introduction of ¹⁹⁸Au colloid for BMS in 1958, many other radiotracers have been used for this purpose. Most early radiotracers were noted to have poor imaging characteristics and/or unfavorable radiation dosimetry.³² However, the introduction of new radiopharmaceuti-

Table 1 Radiotracers for Bone Marrow Imaging

Radiotracers	Dose (mCi)	Principal Photon Energy (keV)	Physical Half-Life	Localization	Liver/Spleen Activity
^{99m} Tc-sulfur colloid	5-15	140	6 h	RES	++++
^{99m} Tc-nanocolloid	10-20	140	6 h	RES	+++
⁵² Fe	0.1-0.2	165, 511	8.2 h	Erythropoietic	No
¹¹¹ In-chloride	2-4	174, 247	2.8 d	Unclear	++
¹¹¹ In-WBC	0.5	174, 247	2.8 d	Probably RES	++
^{99m} Tc-WBC	10-20	140	6 h	Probably RES	++
^{99m} Tc-NSAb	8	140	6 h	Granulopoietic	+
¹⁸ F-FDG	10-15	511	2 h	Active elements	+

cal agents that localize in the bone marrow such as FDG has substantially improved the quality of scintigraphic images that can be generated with PET.

Several radiotracers that are used for BMS (Table 1) have been developed against 3 main targets: (1) the reticuloendothelial system (RES), (2) erythropoietic cells, and (3) granulopoietic cells.^{30,33} The RES can be imaged by use of radiolabeled colloids, erythropoietic marrow activity can be imaged with radioactive iron (⁵²Fe), and several monoclonal antibodies directed against antigens of granulopoiesis have been developed for imaging of the granulopoietic marrow.³⁴⁻³⁹ ¹¹¹In chloride also has been used as a marrow imaging agent, although the exact target cells have not been identified.^{30,33}

At present, ^{99m}Tc-sulfur colloid (SC) is the most commonly used agent in scintigraphy for bone marrow evaluation. These particles are taken up by the RES in the red marrow, liver, and spleen. Because of the smaller particle size, sulfur colloid prepared by the hydrogen sulfide bubbling technique (<100 nm) yields better marrow images than that prepared by acid reduction of sodium thiosulfate (100-1,000 nm). Nanocolloids (^{99m}Tc-microaggregated human serum albumin and ^{99m}Tc-antimony sulfide colloid) demonstrate relative selectivity for bone marrow (15% to 20% of the injected dose) and less hepatic and splenic uptake.^{30,33,40,41} However, it has been reported that these nanocolloids show greater background and greater urinary bladder activity than ^{99m}Tc-SC.

⁵²Fe citrate is physiologically the ideal agent for the assessment of erythropoietic marrow activity.⁴² Unfortunately, it is relatively expensive because it is produced in a cyclotron and requires PET for its optimal utilization. However, the lack of radiotracer uptake in the liver and spleen with this approach allows evaluation of extramedullary hematopoiesis in these organs as well as in the spine.

¹¹¹In binds to transferrin in exactly the same manner as iron but the biological behavior of indium and iron is different (In³⁺ is not reduced like iron to In²⁺ state) in as many respects as they are similar,⁴³ and marrow ¹¹¹In uptake likely reflects the distribution of erythropoietic marrow. Although the mechanism of marrow uptake of this radiotracer is unclear,³⁰ the distribution is similar to that of ^{99m}Tc-SC in patients with normal bone marrow. Many investigators believe that ¹¹¹In is essentially a reticuloendothelial cell agent. Approximately 30% of ¹¹¹In is found in the bone marrow, 20%

in the liver, 7% in the kidneys, 1% in the spleen, and the rest shows nonspecific distribution throughout the body.

^{99m}Tc-HMPAO labeled white blood cells are useful as a good bone marrow imaging tracer. As these granulocytes are damaged during the labeling process and are therefore trapped in the marrow, the images presumably represent the distribution of marrow reticuloendothelial cells. Although there is considerable liver activity with this technique, it is significantly less than that seen with the colloid agents so that the spine is usually minimally obscured.⁴³ However, the labor-intensive cell labeling procedure makes this technique impractical.

Immunoscintigraphy of the bone marrow has been performed with ^{99m}Tc labeled murine monoclonal antibodies (^{99m}Tc-NSAb) directed against nonspecific cross-reacting antigen, which is expressed in the cytoplasm and at the cell membrane of granulocytes in the blood as well as in mature granulopoietic cells in the bone marrow.³⁷⁻³⁹ Granulopoietic bone marrow cells have a concentration ratio of 50 to 100 to 1 excess when compared with granulocytes in the peripheral blood. Therefore, ^{99m}Tc-NSAb distributes primarily to granulopoietic bone marrow after intravenous injection and provides high-quality images. However, increasing hepatic and splenic uptake have been reported after repeated injections of murine monoclonal antibody.

The distributions of the RES and hematopoietic system are similar in healthy individuals and in most disease states, as confirmed by simultaneous imaging with radioactive iron and radiocolloids.^{42,44,45} Therefore, any tracer that targets either of these 2 systems may potentially be used for clinical purposes to evaluate the bone marrow. However, discrepancies in the distributions of the hematopoietic system and the RES have been reported, most often in the setting of aplastic anemia.⁴⁶ This dissociation has not been seen in patients with marrow expansion resulting from hemolytic anemia, and in this setting, radiocolloids appear to be the agents of choice to demonstrate the extent of marrow expansion and the pattern of distribution.

FDG

FDG is a glucose analog, and its whole-body distribution can be imaged by using modern PET instrumentation. After transport into cells by glucose transporters, FDG becomes trapped inside the cells after phosphorylation by hexokinase

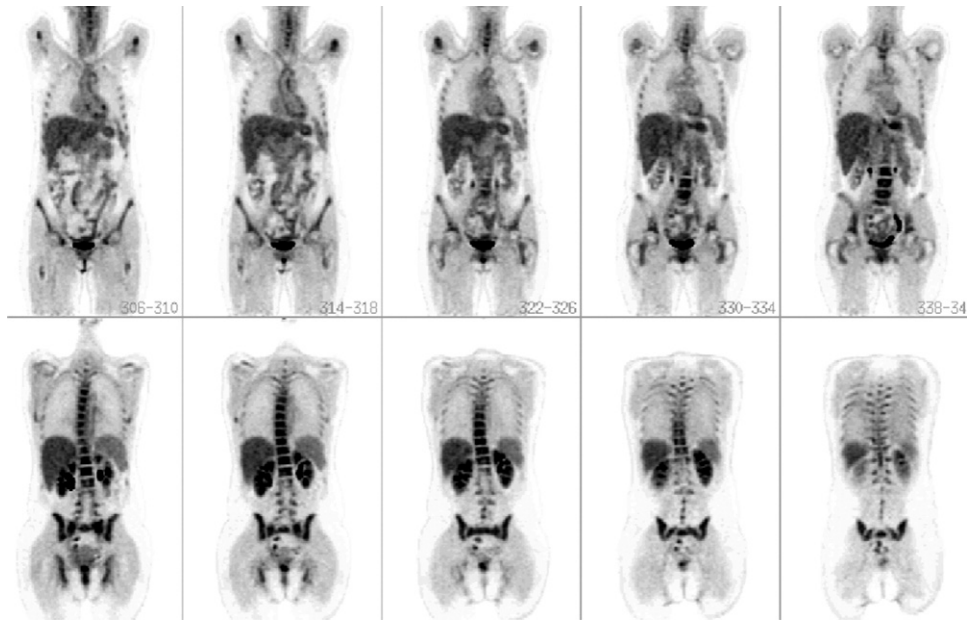


Figure 4 Patient with non-Hodgkin's lymphoma underwent FDG-PET after intense chemotherapy and administration of granulocyte colony-stimulating factor. Whole-body PET images demonstrate diffusely increased uptake in entire skeleton and in spleen due to marrow recovery.

to FDG-6-phosphate. Therefore, FDG can approximate the rate of glycolytic metabolism in both normal and abnormal states. Tumor cells generally have a greater rate of glycolysis as a result of the increased activity of glycolytic enzymes and increased membrane glucose transport. Although FDG is not a bone marrow-specific tracer, it is useful for examination of functioning red marrow as well as for detection of bone marrow involvement by both benign and malignant disorders.⁴⁷

FDG-PET allows one to detect lesions directly based on the degree of metabolic activity rather than on the alteration of structure, which is in contrast to bone marrow imaging using other tracers that typically demonstrate uptake in normally functioning bone marrow and decreased uptake in sites of disease whether currently active or not. PET/CT provides the synergistic advantages of precise anatomic localization of radiotracer uptake, high contrast and spatial resolution, and accurate quantification of metabolic activity at sites of radiotracer uptake.⁴⁸⁻⁵² Uptake of FDG in the skeleton is caused by active hematopoietic marrow, and its pattern and amount can vary with age and with the level of marrow function at the time of PET examination.⁵²

Cytokine therapy-induced hypermetabolic bone marrow and extramedullary hematopoiesis in the spleen has been reported with many agents, including ^{99m}Tc-SC, ^{99m}c-methylene diphosphonate (MDP), ²⁰¹Tl-chloride, ⁶⁷Ga-citrate, and FDG-PET scan imaging.⁵³⁻⁵⁵ Diffusely increased bone marrow uptake on FDG-PET as the result of this condition can simulate generalized bone marrow metastatic disease. However, the timing of the FDG-PET study is of value in differentiating these 2 conditions. In general, the metabolic rate of the bone marrow rapidly will decrease 3 to 5 days after cessation of cytokine therapy, although it can remain higher than baseline for up to 4 weeks.⁵⁶ The increased background

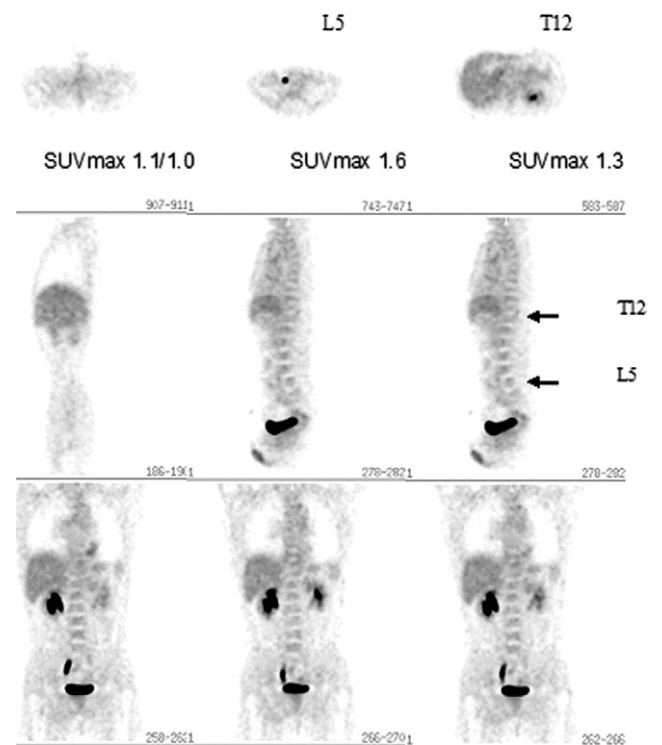


Figure 5 A 38-year-old man with a history of recently diagnosed brain tumor. Upper, middle, and lower rows show axial, sagittal, and coronal slices, respectively, of whole-body FDG-PET scan. Left, middle, and right columns of upper row are at proximal femora, L5 vertebral, and T12 vertebral levels, respectively. Regions of interest were drawn over sites of corresponding axial slices visualized in field of view, and the respective SUVs were calculated.

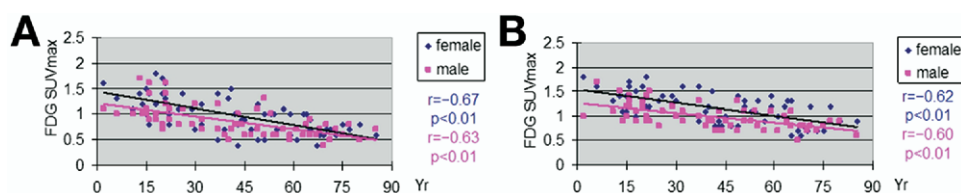


Figure 6 (A) and (B) demonstrate changes in SUV_{max} of proximal femoral and humeral red marrow, respectively, on FDG-PET imaging in relation to increasing age for women and men. There was no significant difference of FDG uptake between red marrow of bilateral humeri or bilateral femora, or between red marrow of males and females ($P > 0.05$, ns). SUV_{max} in extremities declined significantly with advancing age.

uptake of FDG in the bone marrow associated with cytokine therapy can make assessment of focal marrow metastases and their response to treatment difficult (Fig. 4). Consequently, it has been suggested that FDG-PET be delayed for at least 5 days after completion of cytokine therapy when FDG uptake in bone marrow is more likely to return to near baseline levels.⁵⁷

Assessment of Aging Effects on Bone Marrow Metabolism Using FDG-PET

After we obtained institutional review board approval for retrospective data collection and image analysis, along with a HIPAA waiver from the Hospital of the University of Pennsylvania, we retrospectively examined 112 subjects (56 men, 56 women; mean age, 40 ± 20 years, age range, 2-85 years) to determine age-related changes that occur in the red marrow with regard to its distribution and the degree of its metabolic activity by whole-body FDG-PET. These 112 subjects were classified into 8 age categories with equal gender distribution in each as follows: 0 to 15 years (12 subjects), 16 to 25 years ($n = 20$), 26 to 35 years ($n = 10$), 36 to 45 years ($n = 20$), 46 to 55 years ($n = 14$), 56 to 65 years ($n = 16$), 66 to 75 years ($n = 14$), and 76 to 85 years ($n = 6$). Whole-body FDG-PET images were performed at 60 minutes after the intravenous administration of $140 \mu\text{Ci/kg}$ (5.18 MBq/kg) of FDG by using a dedicated whole-body PET scanner. Maximum standard uptake values (SUV_{max}) were calculated from the axial sections of the upper thirds of the humeri and femora, manubrium of the sternum, 12th thoracic and 5th lumbar vertebrae, and anterior superior iliac crests of the pelvis. All available results from other imaging examinations (MRI, CT, and conventional radiography), laboratory data, biop-

sies, and the clinical course of these subjects were reviewed to make certain that the bone marrow sites examined were free of any known pathologies.

There was no significant difference of SUV_{max} in the red marrow activity and distribution between men and women in the same age group ($P > 0.05$, ns) of the entire population. Also, there was no significant difference of SUV_{max} between the red bone marrow of either humeri or femora and of the anterior superior iliac crests of either side ($P > 0.05$, ns; Fig. 5). SUV_{max} values in the extremities declined significantly with advancing age (range of $r = -0.60$ to -0.67 , $P < 0.01$; Fig. 6). However, the SUV_{max} in the axial bone marrow including the manubrium, 12th thoracic and fifth lumbar vertebrae, and anterior superior iliac crests demonstrated a weak correlation with advancing age (range $r = -0.28$ to -0.48 , $P < 0.05$; Fig. 7).

This is the first endeavor to provide information about the functioning bone marrow using whole-body FDG-PET. To our knowledge, no other report in the literature has described typical patterns of physiological distribution of the marrow in the human skeleton by using FDG-PET, or has assessed the changes in red marrow that occur with normal aging over a wide age range. However, there are a few limitations to our study. Although we had adopted exclusion criteria of no chemotherapy for 3 months before imaging and a lack of detectable bone marrow involvement by malignancy, these subjects were to known to have cancer and therefore cannot be considered to be completely normal. In addition, there were only two subjects below the age of 10 years in our study sample, which limits the data we were able to obtain from individuals in this decade of life. Therefore, there is room for further prospective studies to evaluate the bone marrow using FDG-PET in larger populations among all age groups.

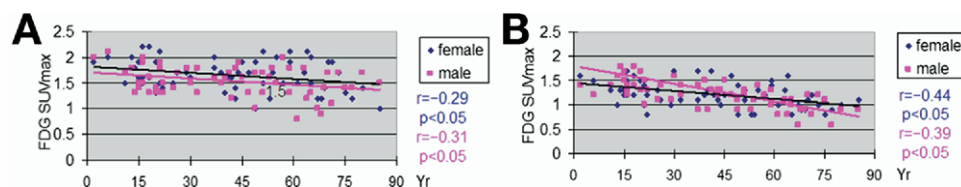


Figure 7 (A) and (B) demonstrate changes in SUV_{max} of axial skeleton red marrow of anterior superior iliac crest and L5 vertebra, respectively, on FDG-PET imaging in relation to increasing age for women and men. There was a statistically significant but weakly correlated trend of decreasing SUV_{max} in red marrow of these sites with increasing age.

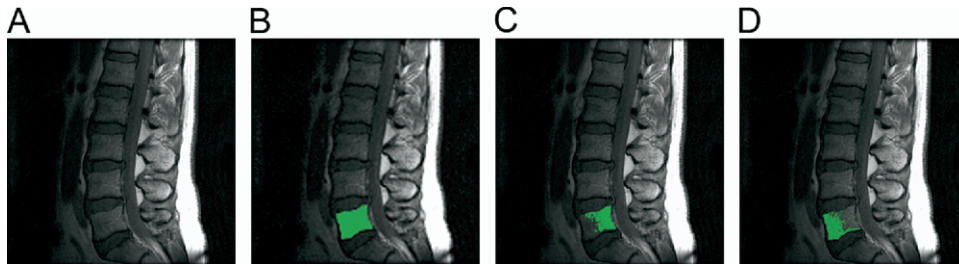


Figure 8 Bone marrow segmentation using sagittal T1 MRI images (A). Tracing of the interior of the vertebral body (B). Segmented yellow marrow by using a threshold interval (C), then subtracting (A) from (B) to obtain a segmentation of the red marrow (D).

Use of Bone Marrow Segmentation on MRI for Quantitative Calculation of Red Marrow Metabolism Using FDG-PET

We retrospectively examined 5 subjects (2 men, 3 women, age 55 ± 6 years) who underwent both MRI and FDG-PET to introduce a new concept for measuring the global metabolic activity of the red marrow. This concept is based on the combination of volumetric segmentation data from structural imaging techniques such as MRI and quantitative metabolic information provided by functional modalities such as PET. In all 5 subjects, MRI of the lumbar spine revealed no abnormalities and FDG uptake was homogenous in the lumbar bone marrow. The mean blood glucose level was 96 ± 25 mg/dL.

The vertebral volume at L1, L3, and L5 were calculated from the available MRI studies. The red and yellow marrow were segmented within the lumbar vertebrae using a novel technique developed in our department (Fig. 8) and their volumes were also calculated.⁵⁸ The mean standardized uptake values (SUV_{mean}) for the bone marrow were calculated in the lumbar spine, and global red marrow activity was calculated through the following: (1) whole vertebral metabolic activity ($WMVA$) = vertebral volume \times SUV_{mean} of the marrow, (2) whole vertebral metabolic activity for yellow marrow ($WMVA_{YM}$) = yellow marrow volume \times SUV_{mean} of fat (obtained from measurements of subcutaneous fat), (3) whole vertebral metabolic activity for red marrow ($WMVA_{RM}$) = $WMVA - WMVA_{YM}$; and finally, (4) metabolic volumetric product (MVP) for red marrow = $WMVA_{RM} \times$ red marrow volume.

The mean volume of the lumbar vertebral body was 15.6 ± 1.4 cm³, the average bone marrow SUV_{mean} was 1.5 ± 0.3 , and the MVP for the lumbar vertebral body was 23.4 ± 5.9 . The mean volume of the yellow marrow in the lumbar vertebral body was 7.7 ± 1.1 cm³, the average yellow marrow SUV_{mean} was estimated to be 0.38 ± 0.1 , and the MVP for the yellow marrow in the lumbar vertebral body was 2.9 ± 0.9 . The mean volume of the red marrow in lumbar vertebral body was 7.9 ± 1.1 cm³, the average red marrow SUV_{mean} was estimated to be 2.6 ± 0.6 , and the MVP for

the red marrow in the lumbar vertebral body was 20.5 ± 5.9 .

These data demonstrate the critical role of modern quantitative techniques such as tissue segmentation for accurate calculation of metabolic activities of complex structures such as bone marrow. These data also demonstrate the importance of partial volume correction using high spatial resolution structural imaging techniques such as MRI to be combined with PET for accurate assessment of metabolic activities of small structures such as red marrow. Furthermore, these measurements will assist in the calculation of global metabolic activities of these tissues in the assessment of normal physiologic as well as pathologic states.

Conclusion

Structural and functional imaging techniques are available to assess the state of the bone marrow in health and in a multitude of benign and malignant disorders. Although the role of structural imaging with MRI has been well established for evaluation of bone marrow, further studies will be necessary to determine the complementary utility of metabolic imaging with FDG-PET as well as other radiotracers. We believe that the combination of these approaches will ultimately enhance the role of medical imaging in the management of primary and secondary marrow disorders.

References

1. Knowles S, Hoffbrand AV: Bone-marrow aspiration and trephine biopsy (2). *BMJ* 281:204-205, 1980
2. Vande Berg BC, Malghem J, Lecouvet FE, et al: Magnetic resonance imaging of the normal bone marrow. *Skeletal Radiol* 27:471-483, 1998
3. Piney A: The anatomy of the bone marrow with special reference to the distribution of the red marrow. *Br Med J* 28:792-795, 1922
4. Politis C, Karamerou A, Block M: Pathophysiologic aspects of the bone/marrow/fat relationship. *Lab Management* 21:40-55, 1983
5. Hashimoto M: Pathology of bone marrow. *Acta Haematol* 27:193-216, 1962
6. Kricun ME: Red-yellow marrow conversion: Its effect on the location of some solitary bone lesions. *Skeletal Radiol* 14:10-19, 1985
7. Vande Berg BC, Lecouvet FE, Moysan P, et al: MR assessment of red marrow distribution and composition in the proximal femur: Correlation with clinical and laboratory parameters. *Skeletal Radiol* 26:589-596, 1997

8. Cristy M: Active bone marrow distribution as a function of age in humans. *Phys Med Biol* 26:389-400, 1981
9. Hartsock RJ, Smith EB, Petty CS: Normal variations with aging of the amount of hematopoietic tissue in bone marrow from the anterior iliac crest. A study made from 177 cases of sudden death examined by necropsy. *Am J Clin Pathol* 43:326-331, 1965
10. Vogler JB 3rd, Murphy WA: Bone marrow imaging. *Radiology* 168:679-693, 1988
11. Baglin TP, Crocker J, Timmins A, et al: Bone marrow hypervascularity in patients with myelofibrosis identified by infra-red thermography. *Clin Lab Haematol* 13:341-348, 1991
12. Lang P, Fritz R, Majumdar S, et al: Hematopoietic bone marrow in the adult knee: Spin-echo and opposed-phase gradient-echo MR imaging. *Skeletal Radiol* 22:95-103, 1993
13. Kaplan PA, Asleson RJ, Klassen LW, et al: Bone marrow patterns in aplastic anemia: Observations with 1.5-T MR imaging. *Radiology* 164:441-444, 1987
14. Poulton TB, Murphy WD, Duerk JL, et al: Bone marrow reconversion in adults who are smokers: MR Imaging findings. *AJR Am J Roentgenol* 161:1217-1221, 1993
15. Fullerton G: *Physiologic Basis of Magnetic Relaxation*. St. Louis, MO, Mosby, 1992
16. Wehrli FW, MacFall JR, Shutts D, et al: Mechanisms of contrast in NMR imaging. *J Comput Assist Tomogr* 8:369-380, 1984
17. Mitchell DG, Burk DL, Vinitzki S, et al: The biophysical basis of tissue contrast in extracranial MR imaging. *AJR Am J Roentgenol* 149:831-837, 1987
18. Parizel PM, Van Riet B, van Hasselt BA, et al: Influence of magnetic field strength on T2* decay and phase effects in gradient echo MRI of vertebral bone marrow. *J Comput Assist Tomogr* 19:465-471, 1995
19. Ricci C, Cova M, Kang YS, et al: Normal age-related patterns of cellular and fatty bone marrow distribution in the axial skeleton: MR imaging study. *Radiology* 177:83-88, 1990
20. Duda SH, Laniado M, Schick F, et al: Normal bone marrow in the sacrum of young adults: differences between the sexes seen on chemical-shift MR imaging. *AJR Am J Roentgenol* 164:935-940, 1995
21. Mitchell DG, Rao VM, Dalinka M, et al: Hematopoietic and fatty bone marrow distribution in the normal and ischemic hip: new observations with 1.5-T MR imaging. *Radiology* 161:199-202, 1986
22. Ishijima H, Ishizaka H, Horikoshi H, et al: Water fraction of lumbar vertebral bone marrow estimated from chemical shift misregistration on MR imaging: Normal variations with age and sex. *AJR Am J Roentgenol* 167:355-358, 1996
23. Kugel H, Jung C, Schulte O, et al: Age- and sex-specific differences in the 1 H-spectrum of vertebral bone marrow. *J Magn Reson Imaging* 13:263-268, 2001
24. Doms GC, Fisher MR, Hricak H, et al: Bone marrow imaging: Magnetic resonance studies related to age and sex. *Radiology* 155:429-432, 1985
25. Dunnill MS, Anderson JA, Whitehead R: Quantitative histological studies on age changes in bone. *J Pathol Bacteriol* 94:275-291, 1967
26. Saifuddin A, Bann K, Ridgway JP, et al: Bone marrow blood supply in gadolinium-enhanced magnetic resonance imaging. *Skeletal Radiol* 23:455-457, 1994
27. Montazel JL, Divine M, Lepage E, et al: Normal Spinal bone marrow in adults: Dynamic gadolinium-enhanced MR imaging. *Radiology* 229:703-709, 2003
28. Sze G, Bravo S, Baierl P, et al: Developing spinal column: gadolinium-enhanced MR imaging. *Radiology* 180:497-502, 1991
29. Daldrup-Link HE, Franzius C, Link TM, et al: Whole-body MR imaging for detection of bone metastases in children and young adults: Comparison with skeletal scintigraphy and FDG PET. *AJR Am J Roentgenol* 177:229-236, 2001
30. Datz FL, Taylor A Jr: The clinical use of radionuclide bone marrow imaging. *Semin Nucl Med* 15:239-259, 1985
31. Kim CK, Reske SN, Alavi A: *Bone marrow scintigraphy, in Nuclear Medicine*. St. Louis, Mosby, 1996, pp 1223-1249
32. Engstedt L, Franzen S, Jonsson L, et al: In vivo localization of colloidal Au198 intravenously injected in polycythemia vera; A preliminary report. *Acta Radiol* 49:66-71, 1958
33. Desai AG, Thakur ML: Radiopharmaceuticals for spleen and bone marrow studies. *Semin Nucl Med* 15:229-238, 1985
34. Noworolska A, Harlozinska A, Richter R, et al: Non-specific cross-reacting antigen (NCA) in individual maturation stages of myelocytic cell series. *Br J Cancer* 51:371-377, 1985
35. Wahren B, Gahrton G, Hammarstrom S: Nonspecific cross-reacting antigen in normal and leukemic myeloid cells and serum of leukemic patients. *Cancer Res* 40:2039-2044, 1980
36. Wahren B, Gahrton G, Ruden U, et al: Clinical evaluation of NCA in patients with chronic myelocytic leukemia. *Int J Cancer* 29:133-137, 1982
37. Munz DL, Sandrock D, Rilinger N: Comparison of immunoscintigraphy and colloid scintigraphy of bone marrow. *Lancet* 336:258-259, 1990
38. Reske SN, Buell U: Reduced technetium 99m labelled NCA-95/CEA-antibody uptake in liver due to gentle antibody reconstitution. Technical note. *Eur J Nucl Med* 17:38-41, 1990
39. Reske SN, Karstens JH, Gloeckner W, et al: Radioimmunoimaging for diagnosis of bone marrow involvement in breast cancer and malignant lymphoma. *Lancet* 1:299-301, 1989
40. Hotze A, Low A, Mahlstedt J, et al: [Combined bone marrow and skeletal scintigraphy in osseous and myelogenous diseases]. *Rofo* 140:717-723, 1984
41. Blend MJ, Pavel DG: Bone marrow imaging: A comparison study using a 99Tcm-sulphur colloid versus a new 99Tcm-microaggregated albumin. *Nucl Med Commun* 7:787-789, 1986
42. Van Dyke D, Price D, Shkurkin C, et al: Differences in distribution of erythropoietic and reticuloendothelial marrow in hematologic disease. *Blood* 30:364-374, 1967
43. Beamish MR, Brown EB: The metabolism of transferrin-bound 111In and 59Fe in the rat. *Blood* 43:693-701, 1974
44. Greenberg ML, Atkins HL, Schiffer LM: Erythropoietic and reticuloendothelial function in bone marrow in dogs. *Science* 152:526-528, 1966
45. Nelp WB, Bower RE: The quantitative distribution of the erythron and the RE cell in the bone marrow organ of man. *Blood* 34:276-282, 1969
46. Fordham E, Amjal A: Radionuclide imaging of bone marrow. *Semin Hematol* 18:222-239, 1981
47. Meyer MA, Nathan CA: Reduced F-18 fluorodeoxyglucose uptake within marrow after external beam radiation. *Clin Nucl Med* 25:279-280, 2000
48. Alavi A, Lakhani P, Mavi A, et al: PET: a revolution in medical imaging. *Radiol Clin North Am* 42:983-1001, 2004
49. Cheran SK, Herndon JE 2nd, Patz EF Jr: Comparison of whole-body FDG-PET to bone scan for detection of bone metastases in patients with a new diagnosis of lung cancer. *Lung Cancer* 44:317-325, 2004
50. Durski JM, Srinivas S, Segall G: Comparison of FDG-PET and bone scans for detecting skeletal metastases in patients with non-small cell lung cancer. *Clin Positron Imaging* 3:97-105, 2000
51. El-Haddad G, Zhuang H, Gupta N, et al: Evolving role of positron emission tomography in the management of patients with inflammatory and other benign disorders. *Semin Nucl Med* 34:313-329, 2004
52. Shreve PD, Anzai Y, Wahl RL: Pitfalls in oncologic diagnosis with FDG PET imaging: Physiologic and benign variants. *Radiographics* 19:61-77; quiz 150-151, 1999
53. Abdel-Dayem HM, Sanchez J, al-Mohannadi S, et al: Diffuse thallium-201-chloride uptake in hypermetabolic bone marrow following treatment with granulocyte stimulating factor. *J Nucl Med* 33:2014-2016, 1992
54. Sugawara Y, Zasadny KR, Kison PV, et al: Splenic fluorodeoxyglucose uptake increased by granulocyte colony-stimulating factor therapy: PET imaging results. *J Nucl Med* 40:1456-1462, 1999
55. Abdel-Dayem HM, Rosen G, El-Zeftawy H, et al: Fluorine-18 fluorodeoxyglucose splenic uptake from extramedullary hematopoiesis after

- granulocyte colony-stimulating factor stimulation. *Clin Nucl Med* 24:319-322, 1999
56. Hollinger EF, Alibazoglu H, Ali A, et al: Hematopoietic cytokine-mediated FDG uptake simulates the appearance of diffuse metastatic disease on whole-body PET imaging. *Clin Nucl Med* 23:93-98, 1998
 57. Mayer D, Bednarczyk EM: Interaction of colony-stimulating factors and fluorodeoxyglucose f(18) positron emission tomography. *Ann Pharmacother* 36:1796-1799, 2002
 58. Udupa JK, Odhner D, Samarasekera S, et al: 3DVIEWSNIX: an open, transportable multidimensional, multimodality, multiparametric imaging software system. *Proc SPIE* 2164:58, 2003